Geologica Acta, Vol.15, Nº 1, March 2017, 25-36, I-X
DOI: 10.1344/GeologicaActa2017.15.1.3

geologica acta

Zircon U-Pb geochronology and emplacement history of intrusive rocks in the Ardestan section, central Iran

F. SARJOUGHIAN[1] A. KANANIAN[2]

[1]Department of Earth Sciences, Faculty of Sciences, University of Kurdistan
Sanandaj, Iran. E-mail: Fsarjoughian2@gmail.com Tel: 00989131005827, Fax: 00988736624133

[2]School of Geology, College of Science, University of Tehran
Tehran, Iran. E-mail: Kananian@khayam.ut.ac.ir

ABSTRACT

The Urumieh-Dokhtar Magmatic Arc (UDMA) is part of the Alpine–Himalayan orogenic belt and interpreted to be a subduction-related Andean-type magmatic arc. Along this belt, Eocene volcanics and some gabbroic to granitic bodies crop out. The main rock types of the studied intrusion are granite, granodiorite, and diorite. They have geochemical features typical of magnesian, calc-alkaline, metaluminous to slightly peraluminous granites and I-type intrusive rock that have a strong enrichment in Large-Ion Lithophile (LIL) elements (*e.g.* Rb, Ba, Sr), and a depletion in High Field Strength (HFS) elements (*e.g.* Nb, Ti, P), typical of subduction-related magmas. Zircon U-Pb dating was applied to determine the emplacement ages of the different intrusions in the Ardestan area. Among them the Kuh-e Dom diorite is 53.9±0.4Ma old; the Kuh-e Dom granodiorite is 51.10±0.4Ma old; the Mehrabad granodiorite is 36.8±0.5Ma old, the Nasrand granodiorite is 36.5±0.5Ma old, the Zafarghand granodiorite is 24.6±1.0Ma old, and the Feshark granodiorite is 20.5±0.8Ma old. These results delineate more accurately the magmatic evolution related to the Neotethyan subduction from the Lower Eocene to Lower Miocene, and the subsequent Zagros orogeny that resulted from the Arabia-Eurasia collision. The emplacement of these intrusive rocks inside the UDMA, which has a close relationship with the collisional orogeny, is transitional from a subduction-related setting to post-collisional setting in the Ardestan area.

KEYWORDS | **Zircon. Geochronology. Ardestan. Urumieh-Dokhtar Magmatic Arc belt. Iran.**

INTRODUCTION

The NW-SE trending Zagros Mountains in Iran are a member of the Alpine-Himalayan orogenic belt and represent one of the youngest continental collision zones on Earth. The Zagros orogeny consists of three NW-SE trending parallel subdivisions from Northwest to Southeast: the Zagros Fold-Thrust Belt (ZFTB), the adjacent Sanandaj-Sirjan Zone (SSZ), and the Urumieh-Dokhtar Magmatic Arc (UDMA) (Alavi, 2004). The tectonic history of the Tethyan region has been studied by many authors (*e.g.* Stöcklin, 1974; Berberian and King, 1981; Mohajjel *et al.*, 2003; Agard *et al.*, 2011). From the Late Precambrian up to the Permian, part of Gondwana was separated from the Eurasian Plate by the Paleo-Tethys. During the Middle to Late Triassic, during the closure of the Paleo-Tethys in the North, rifting in the continental plate along the Zagros thrust zone occurred, resulting in the opening of a new ocean, the Neo-Tethys. During the Triassic–Jurassic, following the closure of Paleo-Tethys, the oceanic crust of Neo-Tethys started to subduct beneath the Eurasian Plate. This subduction progressively closed

the Neo-Tethys ocean and during the terminal collision formed the Zagros orogenic belt of Iran (Berberian and King, 1981; Alavi, 2004).

Volcanism in the UDMA initiated during the Eocene and continued throughout this period (Berberian and King, 1981). Its composition has a common calc-alkaline to shoshonitic and alkaline affinity with geochemical and petrological features similar to those of Andean-type magmatism (*cf.* Berberian *et al.*, 1982). The oldest igneous rocks in the UDMA are the calc-alkaline Shir-Kuh granitic complex, which cut across Upper Jurassic formations and are overlain unconformably by Lower Cretaceous fossiliferous limestone exposed in the southeastern margin of central Iran (Nabavi, 1972; Hajmolla-Ali *et al.*, 2000). The youngest rocks in the UDMA consist of lava flows and pyroclastics which form Pliocene to Quaternary volcanic cones with alkaline to calc-alkaline compositions (Berberian and Berberian, 1981). It is suggested that the Plio-Quaternary volcanism formed as a result of: i) the modification of the geothermal gradients due to uplift and erosion, ii) the strike-slip shearing motion created by differential movement of fault blocks due to the continued convergence of Arabia and Eurasia, and iii) the existence of large strike-slip faults, which developed a region of tension at both ends of these blocks (Berberian and King, 1981).

The collision has been recently studied in terms of geophysics, kinematics, and neotectonics. It is generally admitted that the Neo-Tethyan subduction started during the Triassic in Iran (Berberian and Berberian, 1981; Wilmsen *et al.*, 2009; Chiu *et al.*, 2013). The timing of its ending, and the onset of the Arabia-Eurasia collision, has long been a subject of debate. Timing estimates of the collision varies from ~65 to ~5Ma, based on a wide variety of presumed geologic responses to collision, such as:

i) ophiolite obduction in the Late Cretaceous and coeval development of a foreland basin on the Arabian margin (Berberian and King, 1981; Alavi and Mahdavi, 1994);

ii) late Eocene as based on structural, lithological, and palaeobiogeographical evidences from both sides of the original Arabia-Eurasia suture (Allen and Armstrong, 2008; Allen, 2009);

iii) early to Mid- Miocene transition from marine to non-marine sedimentation (McQuarrie *et al.*, 2003);

iv) late Miocene/Pliocene influx of coarse clastics into the foreland basin, rapid cooling in the Alborz Mountain, and rapid subsidence of the Caspian Sea (McQuarrie *et al.*, 2003);

v) absence of sedimentation during late Eocene-Oligocene in western part of Central Iran, suggesting that the collision began between 35-25Ma, whereas oceanic subduction is still active (Agard *et al.*, 2005);

vi) emplacement of the Kermanshah ophiolite, that was probably an ancient oceanic core produced by large oceanic detachment faults, indicates that final closure of the Neo-Tethys Ocean occurred in the Late Miocene (Ao *et al.*, 2016).

More recently, Ballato *et al.* (2011) proposed a two-stage collision model that involves an initial collision in the Late Eocene and an acceleration of the regional deformation in the Early Miocene.

The precise timing of collision between Arabia and Eurasia is still controversial and the geological history of the magmatic arcs in the Zagros orogenic belts in Iran is still poorly known. The reconstruction of tectonic and magmatic episodes requires a precise knowledge of their radiometric ages and the characterization of the petrogenetic processes. An increasing number of geochronological results has been published in the last decade for various rock units in Iran, whereas radiometric age constraints on the timing of plutonism in the UDMA are scarce. The aim of this study is to constrain the timing of the emplacement of the Kuh-e Dom, Mehrabad, Nasrand, Zafarghand, and Feshark intrusive rocks located in the middle part of UDMA. Achieving this we seek to provide ing clues about the geodynamic history of the Ardestan magmatic segment, to address some of the most important questions regarding the genesis of the intrusive rocks in the UDMA.

GEOLOGICAL OVERVIEW

Kuh-e Dom

The Kuh-e Dom intrusion, about 40km^2 in size, is located 110km to the northeast of Ardestan in central Iran, and is situated in the eastern part of the UDMA belt (Fig. 1). It can be divided into two main magmatic units, a mafic-intermediate unit and a felsic unit. The mafic-intermediate unit is exposed in the eastern, southern, and northern parts of the felsic unit, forming the marginal parts of the intrusion and includes gabbro-diorites, monzogabbro, monzodiorite, and monzonite. The felsic unit includes granite, granodiorite, and quartz monzonite with associated mafic microgranular enclaves of the same composition as the mafic-intermediate unit (Sarjoughian *et al.*, 2012a; Kananian *et al.*, 2014). The surrounding rocks of the Kuh-e Dom intrusion are mainly Eocene andesitic and rhyolitic lavas, Paleozoic phyllites and schists, and Cretaceous limestones. Paleozoic phyllites and schists are the oldest exposed rocks to the West of the intrusive rocks. The Cretaceous limestones are at its western and

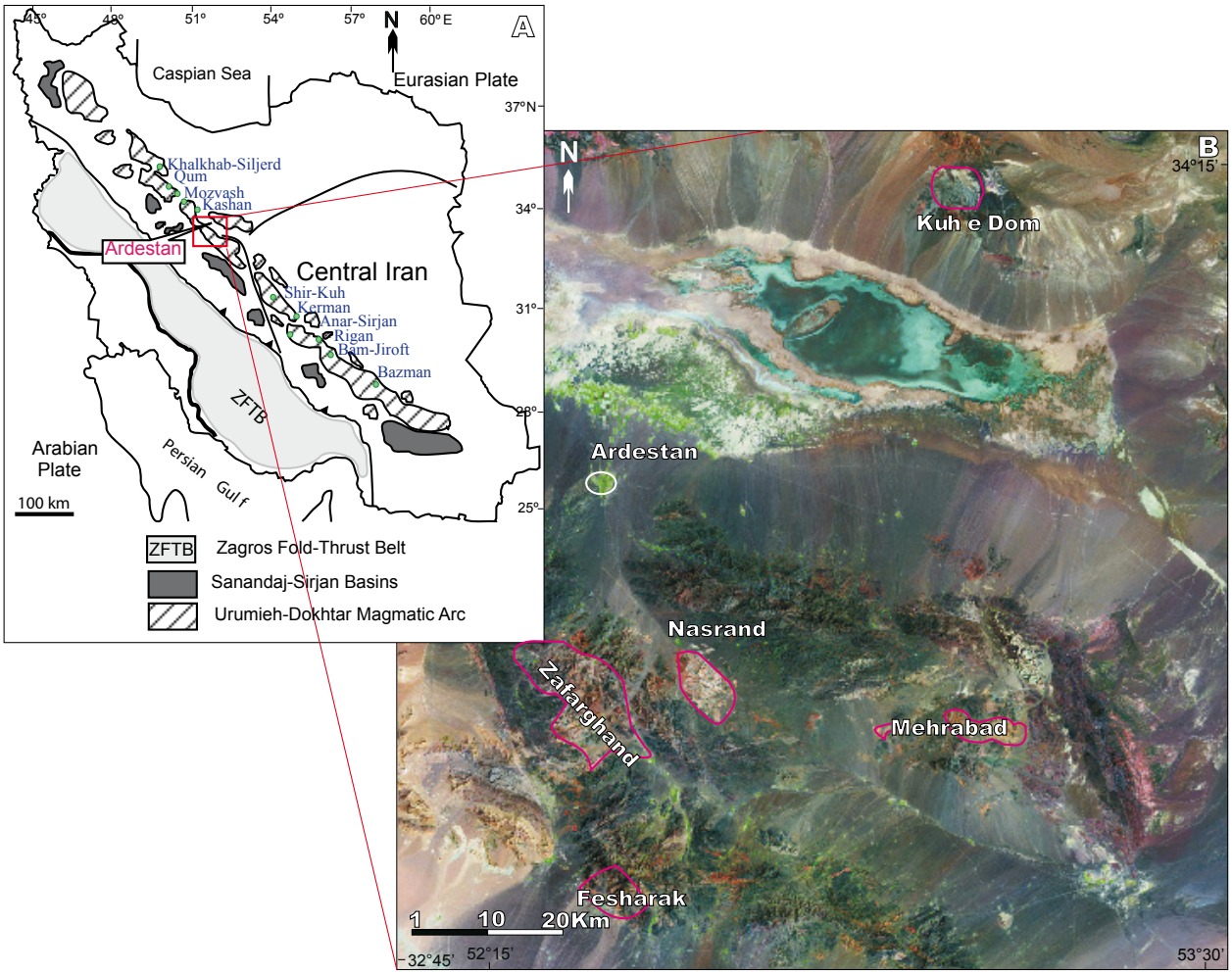

FIGURE 1. A) The location of the study area in a simplified geological map of Iran and B) Location of the studied intrusive rocks plotted onto a satellite image.

southern sides, and the lower Eocene volcanic rocks at its eastern side. The country rocks are altered at the pluton's margins and the contact metamorphosed locally forming skarn and hornfels. The studied intrusion is cut by dikes that can be divided into the following categories: i) felsic dikes, including porphyric microgranite, porphyritic microgranodiorite, and aplite; ii) intermediate-mafic dikes, including phonolite, basanite, and trachyandesite. These dikes have a thicknesses ranging from 50cm up to 20m (Sarjoughian *et al.*, 2012b).

Mehrabad

The Mehrabad intrusion is located in the Southeast of Ardestan, between 33°9'–33°13'N and 52°54'–53°2'E. This intrusion forms an elongated, East-West trending stock-like intrusive mass and crops out in two localities, Sohyle Pakuh at the East side and Hajiabad at the West side (Fig. 1). The Sohyle Pakuh intrusion includes granodiorite and subordinates monzonite and diorite, which may show either gradational or intrusive relations. The Hajiabad intrusion is composed of granodiorite and granite, and less common tonalite that has gradational contacts. An undifferentiated tectonic mélange is the oldest exposed rocks, consisting of spilite, basalt, andesite, radiolarite, and Cretaceous to early Paleocene pelagic sedimentary rocks in contact with the intrusive rocks. Cretaceous *Globotruncana* limestones with chert are interbedded with this mélange zone. The Eocene sequence consists of andesite, dacite, and tuffite cut by intrusive rocks. This extrusive rocks are metamorphosed in the contact with the intrusion and the grade of contact metamorphism is generally within the albite-epidote hornfels facies.

Nasrand

The Nasrand intrusion covers an area of ca. 28km^2 at 52°33'–52°34'E and 33°13'–33°15'N, to the Southeast of Ardestan (Fig. 1). The main rock types are granite and granodiorite, gradually transitioning into granodiorite

along the western margin of the intrusion. The undeformed granitic rocks are generally light grey to pink in color and have an elliptical shape. The granitic rocks intrude older rhyolite, dacite, and andesite rocks of Eocene age; consequently, field relationships indicate a post-Eocene emplacement age. This intrusion is cut by numerous Northeast-Southwest trending dark grey dioritic and gabbroic dikes 50 to 100cm in thickness. The alteration of the intrusion is not strong, with only weak epidotization and chloritization.

Zafarghand

The Zafarghand intrusive rocks are located in the South of Ardestan, between 52°18'E to 52°30E and 33°N to 33°12'N. The studied intrusion is the largest intrusive body in the Ardestan area and forms a markedly elongated body with a NW-SE direction, following an earlier fault trend (Fig. 1). The Zafarghand intrusive rocks include mafic to felsic intrusive bodies ranging in composition from gabbro to diorite, granodiorite and granite. The studied complex intruded Eocene volcanic rocks, including basalt, basaltic andesite, andesite, latite, dacite, rhyolite, and volcaniclastic rocks, such as tuff and ignimbrite. The contact with these volcanic rocks is marked by albite-epidote hornfels to hornblende hornfels facies. Granodiorite is the most abundant lithology followed by diorite. To the Northwest, diorite is transitional to more felsic rocks (granodiorite), while to the Southeast, diorite forms the margin of the pluton. It takes about 50 percent of the pluton and is light grey. Granitic rocks are found in the northern and northwestern parts of the complex and are light cream to white. The contacts between granites and granodiorite are typically gradational, suggesting *in situ* magma differentiation as the main process. Sometimes granites occur as leucocratic dikes or small stocks intruding the granodiorites. Gabbros form the smallest volume of the intrusive rocks in the central zone and are black to dark grey. They are surrounded by granodiorites and diorites with generally sharp contacts. Occurrence of veins of granodioritic magma in the gabbroic rocks, shows that gabbroic rocks are older than granodioritic rocks. Fine-grained, mafic microgranular enclaves, of diorite and quartz diorite composition and 10cm to 2m in length, are enclosed in the granodiorites, preferentially in the central part. The former may show either gradual or sharp contacts with the host granodiorite. Most of these enclaves show chilled margins. They may represent mingling between coeval mafic and felsic magmas. The intrusive rocks are cut by a few porphyritic microgranite, microgranodiorite and aplitic dikes. The dikes generally show subhorizontal orientations, although sometimes they clearly cross cut each other. They range in thickness from a few cm to 1m.

Feshark

The Feshark intrusion is situated in the South of Ardestan (Fig. 1). Its coordinates are 32°50'–32°53'N and 52°21'–52°26'E. It is composed mainly of granodiorite, granite, diorite, and quartz-diorite. Quartz-diorite and diorites are dark grey and abundant in the western part of the intrusion. Granodiorite and granites are typically white to light grey and change gradually into granite, whereas they show a distinct boundary with quartz-diorite and diorites. Because of the occurrence of veins of granitic material in the dioritic rocks, we infer that diorites might have formed at the earlier stage. Granodiorites contain abundant rounded to ellipsoidal mafic microgranular enclaves of diorite and quartz diorite composition. They are 5–50cm in diameter and show chilled margins. Country rocks are Cretaceous and Eocene deposits. Submarine Cretaceous to Eocene deposits are mainly volcanic and volcano-sedimentary rocks, intercalated between deep sea sediments. Volcanic rocks include rhyolite, rhyodacite, trachyandesitic, andesite, and basalt. In the West, sedimentary rocks include *Inoceramus*-bearing limestones with silty marls and sandy limestones, which are metamorphosed near the intrusion contacts. The grade of metamorphism is locally high, from pyroxene hornfels to hornblende hornfels facies, especially along the margin of the western zones of the studied intrusion.

ANALYTICAL TECHNIQUES

Sixty representative samples from the Kuh-e Dom, Mehrabad, Nasrand, Zafarghand, and Feshark were collected on the basis of their mineralogy, freshness, and geographic distribution. The selected samples were analyzed for major and trace elements. Major elements were analyzed by X-ray fluorescence (XRF) (Rigaku RIX 2000 with a Rh end window tube) using fused glass disks at Naruto University in Japan. Glass beads from finely grounded samples were prepared with a sample-to-flux ($Li_2B_4O_7$) ratio of 1:10 and analyzed for major elements using fundamental parameter method spectrometry with analytical errors <1%.

Six representative samples for U-Pb zircon dating were collected from the Kuh-e Dom (granodiorite and diorite), Mehrabad (granodiorite), Nasrand (granodiorite), Zafarghand (granodiorite), and Feshark (granodiorite) intrusions. The samples were 3–7kg in weight. Whole rock samples were crushed using jaw crushers. The crushed samples were then sieved to obtain the size fraction above 53 mesh (~300μm). All samples were washed with water to remove dust. After washing and drying, magnetic minerals, such as magnetite, were removed with a Franz magnetic separator. More than 100 zircon grains were separated

from the samples by using standard mineral-separation techniques at University of Tehran, specifically heavy liquid (bromoform and methylene iodide), and finally purified by handpicking under a binocular microscope.

Zircon separates were mounted by using epoxy resin and polished. Prior to age determination, all zircon grains were investigated by cathodoluminescence (CL) to highlight zoning and possible inherited cores. U-Pb isotopic analyses of zircon were conducted by laser ablation inductively coupled plasma-mass spectrometry (LA ICP-MS) at the State Key Laboratory of Geological Processes and Mineral Resources, China University of Geosciences, Wuhan (see Simonetti *et al*., 2006). Detailed operating conditions for the LA system and the ICP-MS instrument and data reduction were the same described by Liu *et al*. (2008, 2010a, 2010b).

Zircon 91500 was used as external standard for U-Pb dating, and was analyzed twice every five analyses. Time-dependent drifts of U-Th-Pb isotopic ratios were corrected using a linear interpolation (with time) for every five analyses according to the variations of zircon 91500 (*i.e*. 2 zircon 91500 + 5 samples + 2 zircon 91500) (Liu *et al*., 2010a). Preferred U-Th-Pb isotopic ratios used for zircon 91500 were from Wiedenbeck *et al*. (1995). Uncertainty of preferred values for the external standard zircon 91500 was propagated to the ultimate results of the samples. Concordia diagrams and weighted mean calculations were made using Isoplot/Ex_ver3 (Ludwig, 2003).

PETROGRAPHY

Felsic rocks in the Kuh-e Dom, Mehrabad, Nasrand, Zafarghand, and Feshark intrusions, are mostly granular, medium grained and composed mainly of quartz, K-feldspar, plagioclase, biotite, and hornblende, with small amounts of accessory minerals, including zircon, apatite, titanite, as well as opaque minerals, such as magnetite, hematite, pyrite, and chalcopyrite. Quartz and K-feldspar are typically anhedral and occur as interstitial phases. Occasionally, K-feldspar phenocrysts are present as large, irregular, poikilitic patches. They enclose fine-grained plagioclase, hornblende, biotite, and accessory minerals. Plagioclase occurs as euhedral to subhedral crystals with zoning or polysynthetic twinning. Plagioclase tends to be an early, dominant phase. Green hornblende and brown biotite are common mafic minerals and form euhedral to subhedral prisms of variable size.

The mafic-intermediate rocks in these intrusions are granular and medium grained; they contain more mafic minerals and plagioclase, and less quartz and K-feldspar compared to the granodiorite rocks. Quartz and orthoclase are present in variable proportions. Both minerals are commonly late interstitial phases. Plagioclase occurs as euhedral to subhedral crystals, commonly with polysynthetic twining and normal and oscillatory zoning. Hornblende and biotite are the most common mafic minerals, whereas in the mafic units orthopyroxene occurs as rare grains in the Kuh-e Dom and Zafarghand intrusions and forms euhedral to anhedral crystals and usually contains small inclusions of plagioclase. Apatite, titanite, and opaque minerals (mostly titanomagnetite, hematite, pyrite, and chalcopyrite) appear as accessory phases.

GEOCHEMICAL COMPOSITION

Whole-rock analyses of major and trace elements of all samples are reported in Table I (Electronic Appendix, available at www.geologica-acta.com). We use the classification diagram of Middlemost (1994) for characterizing the rock types. The samples plot in the fields of gabbro to granite (Fig. 2). The majority of the samples are subalkaline in nature and display a calc-alkaline trend (Irvine and Baragar, 1971; Fig. 3A). In the FeO/(FeO+MgO) *vs*. SiO_2 diagram (Frost *et al*., 2001), all samples plot in the magnesium field (Fig. 3B). The A/CNK [Al_2O_3/(CaO+Na_2O+K_2O) molecular ratio, or Aluminum Saturation Index (ASI)] values of Shand (1943), are the most useful chemical discriminant between metaluminous (ASI<1) and peraluminous (ASI>1) intrusive rocks; the vast majority of the studied intrusion are metaluminous to slightly peraluminous (Fig. 3C). The least-evolved members are predominantly metaluminous, although some more evolved samples exhibit slightly peraluminous signatures with A/CNK ratios ranging from 1.0 to 1.1. The

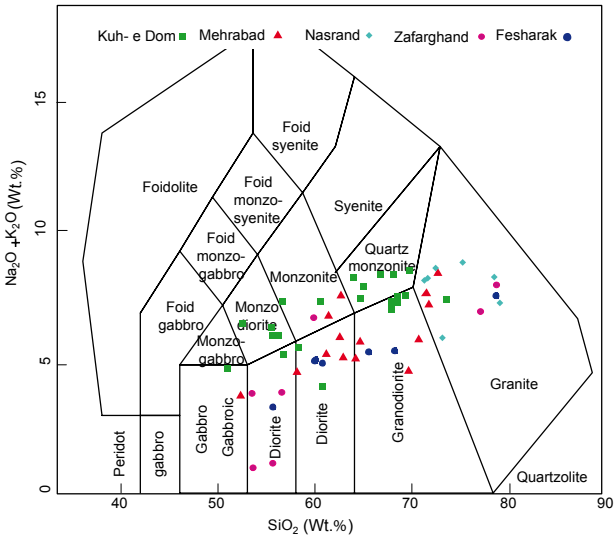

FIGURE 2. Silica *vs*. alkali diagram (Middlemost, 1994), showing the studied samples plotted in the fields from granite to gabbro.

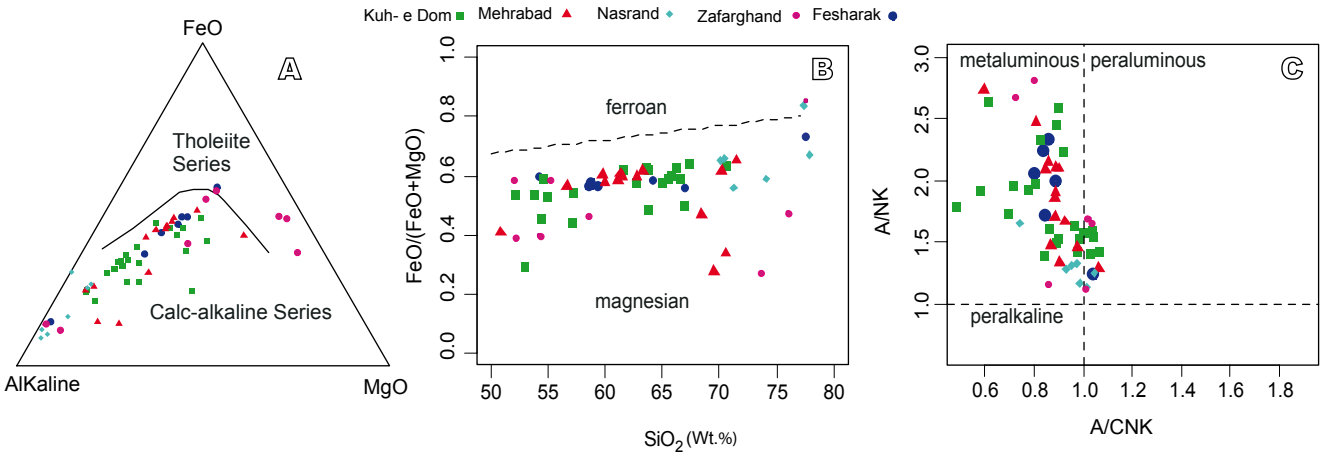

FIGURE 3. A) Alkaline ternary diagram (Na_2O+K_2O-FeO-MgO; wt.%). Line separating the tholeiitic and calc-alkaline fields is from Irvine and Baragar (1971), B) SiO_2 *vs.* Fe/(FeO+ MgO) diagram (Frost *et al.*, 2001), and C) $[Al_2O_3/(CaO+Na_2O+K_2O)]$mol *vs.* $[Al_2O_3/(K_2O+Na_2O)]$mol diagram (Shand, 1943) for the granites of the Ardestan area.

ASI value of the studied samples is less than 1.1, which is associated mainly with I-type granites (Chappell and White, 1974; Chappell, 1999). Low ASI is consistent with the mafic mineral assemblage of amphibole±pyroxene±biotite in the studied samples (Chappell and White, 1974; White and Chappell, 1988). The peraluminous nature of a few samples may be attributed to hornblende differentiation (Zen, 1986) or heterogeneity of water content in the protolith (Waight *et al.*, 1998).

A discrimination plot of Zr+Ce+Y+Nb *vs.* (Na_2O+K_2O)/CaO and FeOt/MgO (Whalen *et al.*, 1987) shows that the studied samples plot within the field of I- and S-type intrusive rocks and are distinct from the A-type granites of alkali nature (Fig. 4). The sharply linear negative trend between P_2O_5 and SiO_2 (Chappell, 1999) and sharply linear positive trend between Th and SiO_2 from the most mafic to the most felsic compositions (Chappell *et al.*, 1998) can be considered typical of I-type granite (Fig. 5). The oxidized I-type geochemical signatures of these intrusive rocks are also supported by their mineralogy, *i.e.* predominance of biotite and hornblende as mafic silicates, and the abundance of euhedral titanite and magnetite as accessory phases (Chappell and White, 1974). Lack of muscovite and monazite minerals is typical of I-type intrusive rocks. Apatite inclusions are common in biotite and hornblende, as are expected for I-type intrusive rocks and occur in larger individual crystals in the S-type varieties. The wide range of modal distribution from gabbro to granite, indicates the studied samples are I-type granitoids.

In the Mid Oceanic Ridge Basalt (MORB) normalized trace-element spider diagrams (Pearce, 1983), the five groups of intrusive rocks have similar trace-element patterns

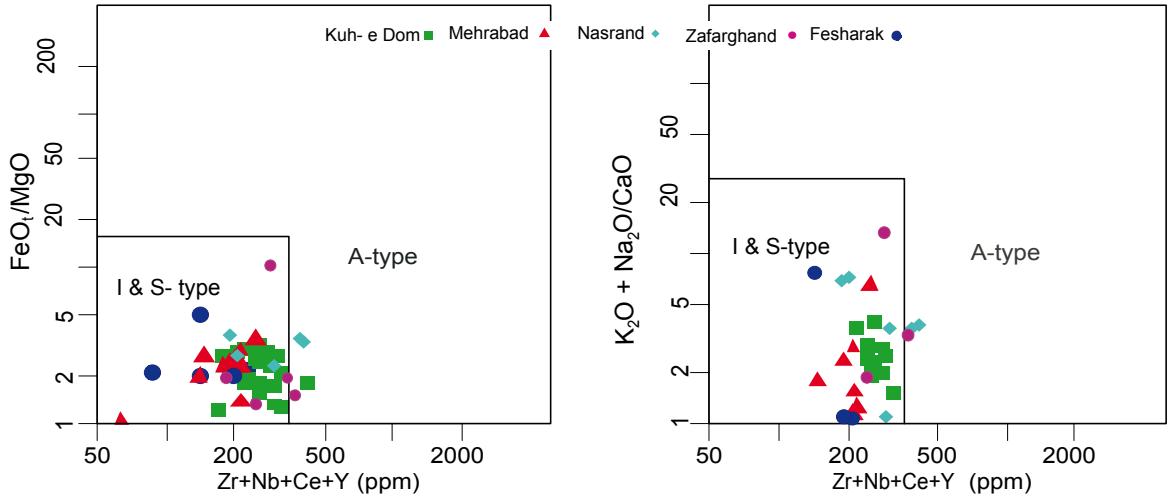

FIGURE 4. Zr+Ce+Y+Nb *vs.* (Na_2O+K_2O)/CaO and FeO_t/MgO discrimination diagrams of Whalen *et al.* (1987).

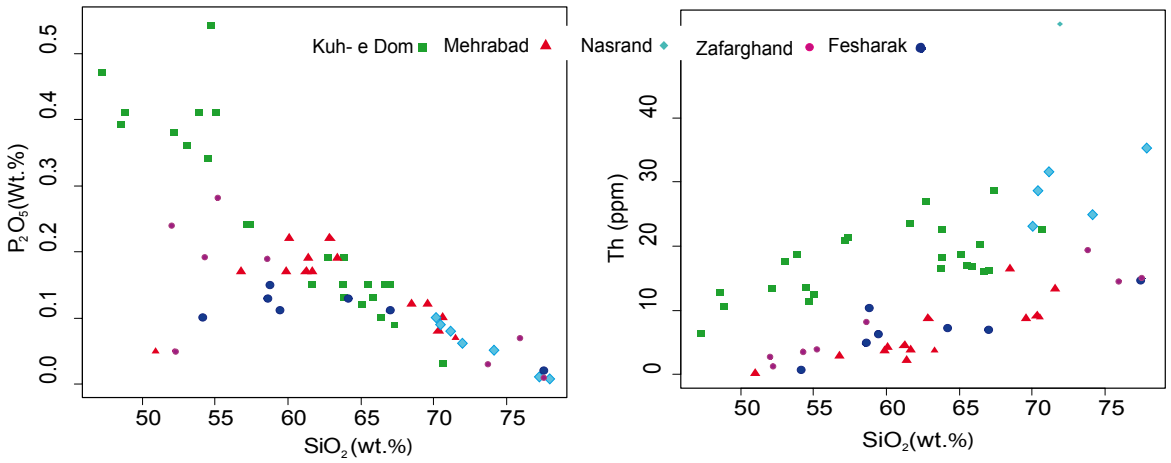

FIGURE 5. SiO_2 *vs.* P_2O_5 and Th diagrams indicating typical trends of I-type granite.

(Fig. 6). These rocks are enriched in Large Ion Lithophile Elements (LILEs: Cs, Rb, Ba, and K) and strongly depleted in High Field Strength Elements (HFSEs: Nb and Ti). These features are typical of subduction-related magmas (Gill, 1981; Pearce, 1983; Wilson, 1989). Strong depletion in Nb and Ti relative to other HFSE has been explained in terms of: i) retention of Nb-Ti-bearing refractory phases (*i.e.* rutile, titanite, amphibole) at the site of partial melting (*e.g.* Briqueu *et al.*, 1984); ii) melting of Nb-Ti-depleted source material, be it continental crust, island arc, or continental margin volcanic rocks; iii) recycling of ancient crustal material back into the mantle sources of magmas (*e.g.* Hergt *et al.*, 1989; Sage *et al.*, 1996); iv) metasomatized mantle wedge of volcanic arcs (Taylor and McLennan, 1985); and v) advanced fractional crystallization of Nb-Ti-bearing phases (ilmenite, titanite, etc.), while the negative P anomalies should result from apatite fractionation. In the Rb *versus* Y + Nb diagram (Pearce *et al.*, 1984; Fig. 7), all the samples display geochemical characteristics typical of I-type magmas, formed in a volcanic arc setting, due to their relatively low values of Nb and Y (see Aliashrafzadeh, 2013; Ghahramani, 2013; Hamzehie, 2013).

ZIRCON U-Pb AGE DETERMINATION

One diorite sample from Kuh-e Dom (DK), and five granodiorite samples from Kuh-e Dom (GK), Mehrabad (MH), Nasrand (NS), Zafarghand (ZF), and Feshark (FS) were selected for zircon U-Pb geochronology (see U-Pb data in Table II). Zircon is a common accessory mineral in the studied rocks and forms prismatic crystals with a maximum size close to 300µm. The zircon crystals are automorphic to sub-idiomorphic, and display a well-developed oscillatory zoning indicative of growth under magmatic conditions (Koschek, 1993; Gao *et al.*, 2007). Zircon is a reliable recorder of magmatic conditions in which it grew, because of its resistance to isotopic resetting at magmatic conditions and its ubiquitous presence in silicic magmas. In a few samples the occurrence of xenocrystic cores can be observed. To determine the age of emplacement of the granites in these samples, analyses were mostly carried out on the external domains of the zircons grains with magmatic textures.

Zircon grains have variable Th and U concentrations (Table II). Generally, a zircon with a Th/U ratio larger than 0.5 and positive correlation between Th and U is regarded as being derived from magmatic crystallization, while if the ratio is less than 0.1 it can be interpreted as metamorphic in origin (Belousova *et al.*, 2002). In this study, their Th/U ratios (Table II) are interpreted as being representative of magmatic zircon. This interpretation is supported by the zircon shapes and textures; and by the positive correlation between Th and U (Fig. 8), that indicate a magmatic origin for these zircons (Hoskin and Black, 2000; Belousova *et al.*, 2002; Xie *et al.*, 2006).

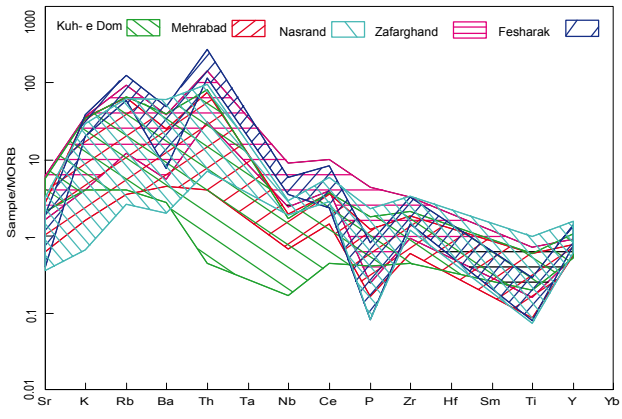

FIGURE 6. MORB-normalized trace patterns for the studied samples (values from Pearce, 1983).

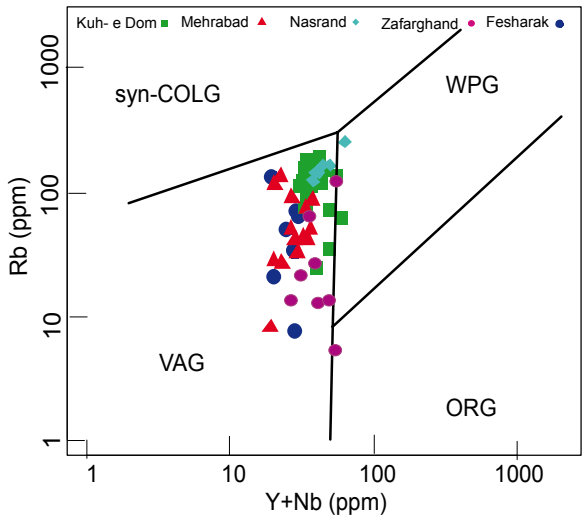

FIGURE 7. Trace-element geotectonic discrimination diagram (Pearce *et al.*, 1984) for the studied granites. The granites plot in the volcanic arc granite field.

The results of calculating the isotopic age of the Kuh-e Dom granodiorite (GK), Kuh-e Dom diorite (DK), Mehrabad granodiorite (MH), Nasrand granodiorite (NS), Zafarghand granodiorite (ZF), and Feshark granodiorite (FS) are presented as concordia and average age graphics (Fig. 9) and the results are given in Table III. Therefore, the U-Pb zircon ages indicate that the Kuh-e Dom diorite and granodiorite were formed during the early to middle Eocene (Ypersian), the Mehrabad and Nasrand granodiorite during the late Eocene (Priabonian), the Zafarghand granodiorite during the late Oligocene (Chattian), and the Feshark granodiorite during the early Miocene (Burdigalian). Therefore, the plutonic rocks in the Ardestan magmatic segment reveal three main episodes of plutonic activity in the early-middle-late Eocene, late Oligocene, and early Miocene.

DISCUSSION

This study reports zircon LA ICP-MS U-Pb ages for the Ardestan intrusive rocks, emplaced in the central part of the UDMA. It is generally believed that the UDMA was overlying the subducting slab of the Neo-Tethyan oceanic lithosphere beneath the Iranian Plate (Berberian and King, 1981; Mohajjel *et al.*, 2003; Agard *et al.*, 2005). Geochemical studies indicate that these intrusions are oxidized I-type, metaluminous to slightly peraluminous, commonly attributed to the magnesian series of calc-alkaline nature, and formed in a subduction-related setting, in accordance with the geological history of this area and in good agreement with other UDMA signatures.

According to our U–Pb results, the granodiorite and diorite of the Kuh-e Dom intrusion were emplaced at 51-54Ma, during the early-middle Eocene, which is slightly older than previous dating by K-Ar (Technoexport, 1981), which yielded late Eocene ages. According to field observations, the intrusive rocks of Mehrabad, Nasrand, Zafarghand, and Feshark, in the Ardestan area, are intruded into early Eocene volcanic rocks (andesite, dacite latite, and tuffs), thus indicating a post-early Eocene age, in agreement with an Oligo-Miocene age estimated earlier (*e.g.* Aghanabati, 2004). The new isotopic data provide a revised age for these intrusive rocks, from the late Eocene (Mehrabad and Nasrand), in contrast with the earlier views, to late Oligocene (Zafarghand), to early Miocene (Feshark). Therefore, the Tertiary plutonism in the Ardestan area can be divided into three main episodes; i) early-middle-late Eocene, ii) late Oligocene and iii) early Miocene intrusions, which have been considered central part of the UDMA plutonism. The intrusive rocks in the Ardestan area were emplaced from early Eocene to early Miocene plutonic interval and the Zafarghand and Feshark intrusive rocks, which are closer to the trench, are the younger intrusive units in the Ardestan area. It is apparent that the plutonism was more intense during the Eocene for the central part of the UDMA belt, as shown also by Berberian and Berberian (1981).

The geochronologic data of the intrusive rocks studied here were compared with those available of plutonic rocks elsewhere in the UDMA. The overall data are listed in Table IV.

Chiu *et al.* (2013) suggested that magmatism in the UDMA was most active and widespread in the Eocene and

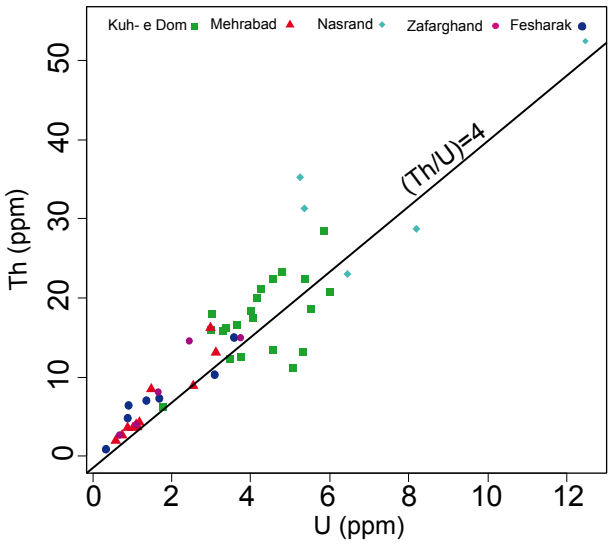

FIGURE 8. The positive correlation between Th and U, indicating a magma origin of zircons.

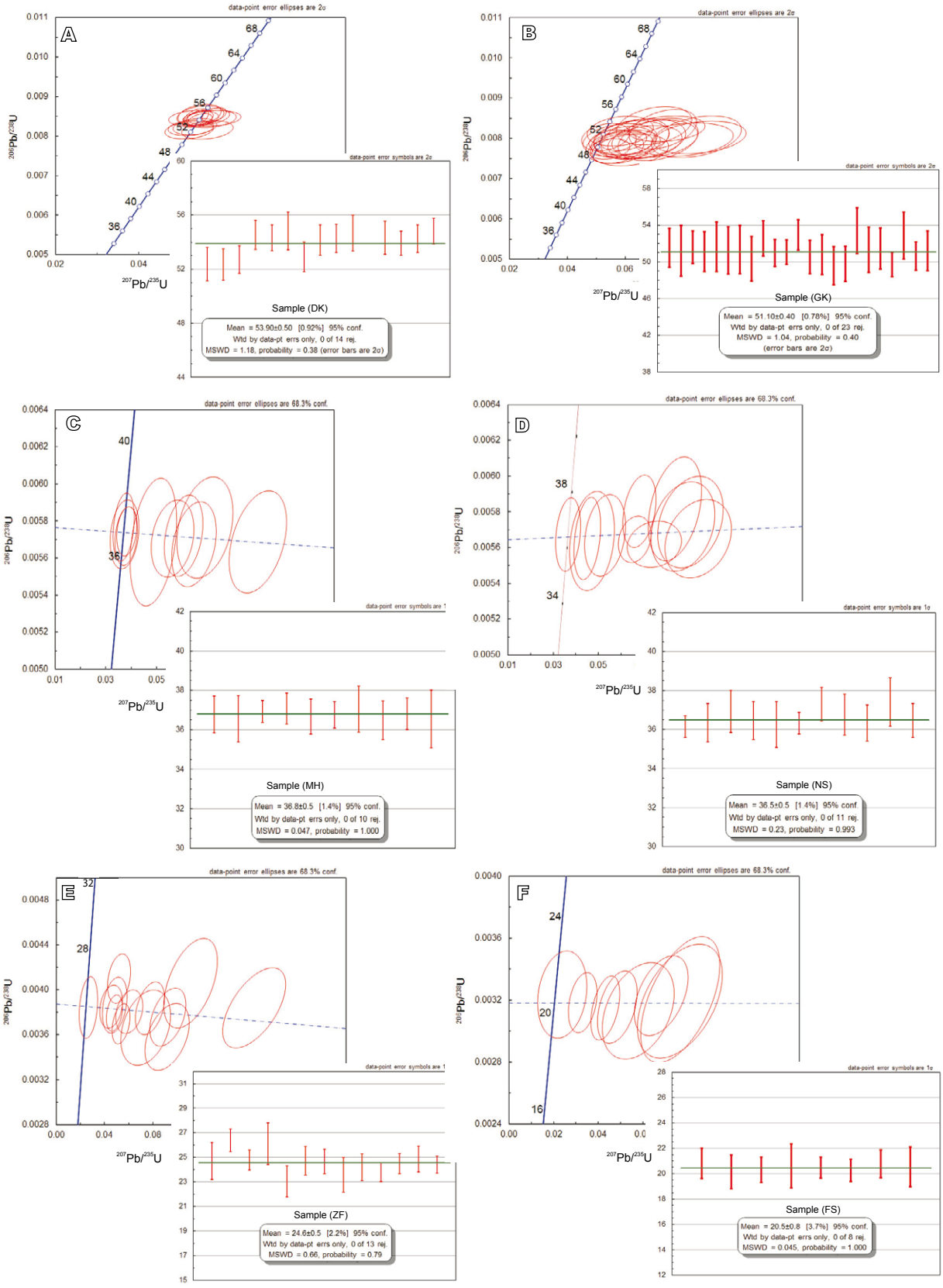

FIGURE 9. Concordia diagrams displaying U-Pb data from A) the Kuh-e Dom diorite, B) Kuh-e Dom granodiorite, C) Mehrabad granodiorite, D) Nasrand granodiorite, C) Zafarghand granodiorite and D) Feshark granodiorite.

Oligocene, and magmatic activity lasting from ca. 21 to 6Ma ending with small-volume intrusions. Cessation of arc magmatism took place progressively from the Northwest to the southeast. This southeastward termination of the UDMA magmatism is consistent with the notion of oblique and thus diachronous collision between Arabia and Eurasia, with the collision initiating in the Northwest and propagating progressively to the Southeast along the Zagros suture zone (see Chiu *et al*., 2013).

From a geochronological point of view, the Aredestan intrusive rocks are broadly similar to the other intrusive rocks in the UDMA spanning from 81.0 to 5.4Ma. This semi-continuously activity all along the UDMA can be related to the persistent subduction of the Neo-Tethys oceanic crust below the Iranian plate. The Kuh-e Dom, Mehrabad, Nasrand, and Zafarghand were emplaced during the Eocene-Oligocene epoch during the maximum magmatic activity. Another phase of plutonism in the Ardestan area was responsible for the emplacement of the Feshark intrusive rocks. Considering most of the researchers agree that the timing of the continental closure is Miocene (*e.g*. Dewey and Sengör, 1979; Robertson, 2000; McQuarrie *et al*., 2003; Mohajjel *et al*., 2003; Homke *et al*., 2004; Guest *et al*., 2006; Omrani *et al*., 2008; Ao *et al*., 2016). It seems that the Eocene-Oligocene intrusive rocks (*i.e*. Kuh-e Dom, Mehrabad, Nasrand, and Zafarghand) in the Ardestan area were emplaced prior to the collision, showing a pre-collisional volcanic arc setting, and that the younger intrusion (*e.g*. Feshark) was formed relatively late in the subduction history and may represent post-collisional plutonism.

CONCLUSIONS

The petrological, geochemical, and geochronological study of the Ardestan intrusive rocks reveals important clues to decipher the complex magmatic processes in the central section of the Urumieh-Dokhtar magmatic arc belt. All magmatic phases forming the intrusive rocks of the Ardestan area were metaluminous to slightly peraluminous, typical of I-type granites and belong to magnesian series of calc-alkaline nature and display the geochemical characteristics typical of oxidized I-type volcanic arc granitoids.

The LA ICP-MS U-Pb zircon geochronology of the Aredestan plutonic rocks documents two major intrusive phases. An Eocene-Oligocene subduction-related magmatism formed the Kuh-e Dom, Mehrabad, Nasrand, and Zafarghand intrusive rocks. The youngest lower Miocene Feshark intrusion probably represents post-collision magmatism within the central part of the UDMA belt.

ACKNOWLEDGMENTS

Thanks go to the University of Kurdistan for supporting this project by means of grants provided by the research council (Number: 4.64500; date: 3/11/2015). We are grateful to Prof. K. Zong at China University of Geosciences, who prepared the U-Pb-Th isotopic data. We thank David Lentz for comments on earlier versions of this manuscript. Thanks are extended to Prof. H. Azizi (University of Kurdistan). We acknowledge Prof. Antonio Castro, Laura Rincón, and anonymous reviewers for their constructive comments leading to an important improvement on the manuscript.

REFERENCES

Agard, P., Omrani, J., Jolivet, L., Mouthereau, F., 2005. Convergence history across Zagros (Iran): constraints from collisional and earlier deformation. International Journal of Earth Science, 94, 401-419.

Agard, P., Omrani, J., Jolivet, L., Whitechurch, H., Vrielynck, B., Spakman, W., Monié, P., Meyer, B., Wortel, R., 2011. Zagros orogeny: a subduction-dominated process. Geological Magazine, 148, 692-725.

Aghanabati, S.A., 2004. Geology of Iran (in Persian). Geological Survey of Iran, 606pp.

Alavi, M., 2004. Regional stratigraphy of the Zagros fold-thrust belt of Iran and its proforeland evolution. American Journal of Science, 304, 1-20.

Alavi, M., Mahdavi, M.A., 1994. Stratigraphy and structure of the Nahavand region in western Iran and their implications for the Zagros tectonics. Geological Magazine, 131, 43-47.

Aliashrafzadeh, H., 2013. Petrogenesis of Intrusive Rocks in Mehrabad Region, East of Ardestan (in Persian). MSc Thesis. University of Tehran, 112pp.

Allen, M.B., 2009. Discussion on the Eocene bimodal Piranshahr massif of the Sanandaj-Sirjan zone, west Iran: a marker of the end of collision in the Zagros orogen. Journal of the Geological Society of London, 166, 981-982.

Allen, M.B., Armstrong, H.A., 2008. Arabia–Eurasia collision and the forcing of mid-Cenozoic global cooling. Palaeogeography, Palaeoclimatology, Palaeoecology, 265, 52-58.

Ao, S., Xiao, W., Khalatbari Jafari, M., Talebian, M., Chen, L., Wan, B., Ji, W., Zhang, Z., 2016. U-Pb zircon ages, field geology and geochemistry of the Kermanshah ophiolite (Iran): From continental rifting at 79 Ma to oceanic core complex at ca. 36 Ma in the southern Neo-Tethys. Gondwana Research, 31, 305-318.

Ballato, P., Uba, C.E., Landgraf, A., Strecker, M.R., Sudo, M., Stockli, D.F., Friedrich, A., Tabatabaei, S.H., 2011. Arabia–Eurasia continental collision: insights from late Tertiary foreland-basin evolution in the Alborz Mountains, northern Iran. Geological Society of America Bulletin, 123, 106-131.

Belousova, E.A., Griffin, W.L., O'Reilly, S.Y. Fisher, N.I., 2002. Igneous zircon: trace element composition as an indicator of

source rock type. Contribution to Mineralogy and Petrology, 143, 602-622.

Berberian, F., Berberian, M., 1981. Tectono–Plutonic Episodes in Iran. Geological Survey of Iran, Report, 52, 566-593.

Berberian, M., King, G.C.P., 1981. Towards a paleogeography and tectonic evolution of Iran. Canadian Journal of Earth Sciences, 18, 210-265.

Berberian, F., Muir, I.D., Pankhurst, R.J., Berberian, M., 1982. Late Cretaceous and early Miocene Andean-type plutonic activity in northern Makran and central Iran. Journal of the Geological Society of London, 139, 605-614.

Briqueu, L., Bouganlt, H., Joron, J.L., 1984. Quantification of Nb, Ta, Ti, and V anomalies in magmas associated with subduction zones: petrogenetic implications. Earth and Planetary Science Letters, 68, 297-308.

Chappell, B.W., 1999. Aluminium saturation in I- and S-type granites and the characterization of fractionated haplogranites. Lithos, 46, 535-551.

Chappell, B.W., White, A.J.R., 1974. Two contrasting granite types. Pacific Geology, 8, 173-174.

Chappell, B.W., Bryant, C.J., Wyborn, D., White, A.J.R., Williams, I.S., 1998. High and low temperature I-type granites. Resource Geology, 48, 225-236.

Chiu, H.Y., Chung, S.L., Zarrinkoub, M.H., Mohammadi, S.S., 2013. Zircon U–Pb age constraints from Iran on the magmatic evolution related to Neotethyan subduction and Zagros orogeny. Lithos, 162-163, 70-87.

Dewey, J.F., Sengör, A.M.C., 1979. Aegean and surrounding regions: complex multiplate and continuum tectonics in a convergent zone. Geological Society of America Bulletin, 90, 84-92.

Frost, B.R., Barnes, G.G., Collins, W.J., Arculus, R.J., Ellis, D.J., Frost, C.D., 2001. A geological classification for granitic rocks. Journal of Petrology, 42, 2033-2048.

Gao, F., Xu, W., Yang, D.B., Pei, F.P., Liu, X., Hu, Z.C., 2007. LA-ICP-MS zircon U-Pb dating from granitoids in southern basement of Songliao basin: constraints on ages of the basin basement. Science in China Series D. Earth Sciences, 50, 995-1004.

Ghahramani, F., 2013. Petrogenesis and geochemistry of enclaves in the Feshark intrusion, NE Isfahan (in Persian). MSc Thesis. University of Tehran, 85pp.

Gill, J.B., 1981. Orogenic Andesites and Plate Tectonics. New York, Springer, 390pp.

Guest, B., Axen, G.J., Lam, P.S., Hassanzadeh, J., 2006. Late Cenozoic shortening in the west-central Alborz Mountains, northern Iran, by combined conjugate strike slip and thin-skinned deformation. Geosphere, 2, 35-52.

Hajmolla-Ali, A., Majidifard, M.R., Hajihoseini A., 2000. Geologic map of the Yazd quadrangle. Tehran, Geological Survey of Iran, scale 1: 100,000.

Hamzehie, Z., 2013. Petrogenesis of the Nasrand intrusive Mass, SE Ardestan (in Persian). MSC Thesis. University of Tehran, 115pp.

Hergt, J.M., Chappell, B.W., McCulloch, M.T., McDougall, I., Chivas, A.R., 1989. The geochemistry of Jurassic dolerites from Portal Peak, Antarctica. Contribution to Mineralogy and Petrology, 102, 298-305.

Homke, S., Vergès, J., Garcés, M., Emami, H., Karpuz, R., 2004. Magnetostratigraphy of Miocene-Pliocene Zagros foreland deposits in the front of the Push-e Kush Arc (Lurestan Province, Iran). Earth and Planetary Science Letters, 225, 397-410.

Honarmand, M., RashidnejadOmran, N., Carfu, F., Emami, M.H., Nabatian, G., 2013. Geochronology and magmatic history of a calc-alkaline plutonic complex in the Urumieh–Dokhtar Magmatic Belt, Central Iran: zircon ages as evidence for two major plutonic episodes. Abhandlungen, Neues Jahrbuch für Mineralogie, 190/1, 67-77.

Hoskin, P.W.O, Black, L.P., 2000. Metamorphic zircon formation by solid-state recrystallization of protolith igneous zircon. Journal of Metamorphic Geology, 18, 423-439.

Irvine, T.N., Baragar, W.R.A., 1971. A guide to the chemical classification of the common volcanic rocks. Canadian Journal of Earth Sciences, 8, 523-548.

Kananian, A., Sarjoughian, F., Nadimi, A., Ahmadian, J., Ling, W., 2014. Geochemical characteristics of the Kuh-e Dom intrusion, Urumieh–Dokhtar Magmatic Arc (Iran): Implications for source regions and magmatic evolution. Journal of Asian Earth Sciences, 90, 137-148

Koschek, G., 1993. Origin and significance of the SEM cathodoluminescence from zircon. Journal of Microscopy, 171, 223-232.

Liu, Y.S., Hu, Z.C., Gao, S., Günther, D., Xu, J., Gao, C.G., Chen, H.H., 2008. In situ analysis of major and trace elements of anhydrous minerals by LA-ICP-MS without applying an internal standard. Chemical Geology, 257, 34-43.

Liu, Y., Gao, S., Hu, Z., Gao, C., Zong, K., Wang, D., 2010a. Continental and oceanic crust recycling-induced melt-peridotite interactions in the Trans-North China Orogen: U-Pb dating, Hf isotopes and trace elements in zircons of mantle xenoliths. Journal of Petrology, 51, 537-571.

Liu, Y., Hu, Z., Zong, K., Gao, C., Gao, S., Xu, J., Chen, H., 2010b. Reappraisement and refinement of zircon U-Pb isotope and trace element analyses by LA-ICP-MS. Chinese Science Bulletin, 55, 1535-1546.

Ludwig, K.R., 2003. ISOPLOT 3.00: A Geochronological Toolkit for Microsoft Excel. Berkeley (California), Berkeley Geochronology Center.

McQuarrie, N., Stock, J.M., Verdel, C., Wernicke, B.P., 2003. Cenozoic evolution of Neotethys and implications for the causes of plate motions. Geophysical Research Letters, 30, 6.1-6.4.

Middlemost, E.A.K., 1994. Naming materials in the magma/igneous rock system. Earth-Science Reviews, 37, 215-224.

Mohajjel, M., Fergusson, C.L., Sahandi, M.R., 2003. Cretaceous–Tertiary convergence and continental collision Sanandaj–Sirjan zone Western Iran. Journal of Asian Earth Science, 21, 397-412

Nabavi, M.H., 1972. Geologic map of the Yazd quadrangle. Tehran, Geological Survey of Iran, scale 1:250,000.

Omrani, J., Agard, P., Whitechurch, H., Benoit, M., Prouteau, G., Jolivet, L., 2008. Arc-magmatism and subduction history beneath the Zagros Mountains, Iran: A new report of adakites and geodynamic consequences. Lithos, 106, 380-98.

Pearce, J.A., 1983. Role of the sub-continental lithosphere in magma genesis at active continental margins. In: Hawkesworth, C.J., Norry, M.J. (eds.). Continental Basalts and Mantle Xenoliths. Shiva, Nantwich, 230-249.

Pearce, J.A., Harris, N.B.W., Tindle, A.G., 1984. Trace element discrimination diagrams for the tectonic interpretation of granitic rocks. Journal of Petrology, 25, 956-983.

Rezaei-Kahkhaei, M., Francisco, C.G., Pankhurst, R.J., Esmaeily, D., 2011. Magmatic differentiation in the calc-alkaline Khalkhab-Neshveh pluton, Central Iran. Journal of Asian Earth Sciences, 42, 499-514.

Robertson, A.H.F., 2000. Mesozoic-Tertiary tectonic sedimentary evolution of a south Tethyan oceanic basin and its margins in southern Turkey, In: Bozkurt, E., Winchester, J.A., Piper, J.D.A. (eds.). Tectonics and Magmatism in Turkey and the Surrounding Area. Geological Society of America, 173 (Special Publication), 97-138.

Sage, R.P., Lightfoot, P.C., Doherty, W., 1996. Geochemical characteristics of granitoid rocks from within the Archean Michipicoten Greenstone Belt, Wawa Subprovince, Superior Province, Canada: implications for source regions and tectonic evolution. Precambrian Research, 76, 155-190.

Sarjoughian, F., Kananian, A., Haschke, M., Ahmadian, J., Ling, W., Keqing, Z., 2012a. Magma mingling and hybridization in the Kuh-e Dom pluton, central Iran. Journal of Asian Earth Sciences, 54-55, 49-63

Sarjoughian, F., Kananian, A., Haschke, M., Ahmadian, J., 2012b. Geochemical signature of Eocene Kuh-e Dom shoshonitic dikes in NE Ardestan, central Iran: implications for melt evolution and tectonic setting. Journal of Geosciences, 57, 241-264.

Shand, S.J., 1943. Eruptive rocks. Their genesis, composition, classification, and their relation to ore-deposits with a chapter on meteorite. New York, John Wiley and Sons, 488pp.

Simonetti, A, Heaman, L.M., Chacko, T, Banerjee, N., 2006. In-situ petrographic thin section U-Pb dating of zircon, monazite, and titanite using laser ablation-MC-ICP-MS. International Journal of Mass Spectrometry, 253, 87-97.

Stöcklin, J., 1974. Possible ancient continental margin in Iran. In: Burk, C.A., Drake, C.L. (eds.). The Geology of Continental Margins. Berlin, Springer, 873-887.

Taylor, S.R., McLennan, S.M., 1985. Models of total crustal composition. In: Taylor, S.R., McLennan, S.M., (eds.). The Continental Crust: Its Composition and Evolution. Boston, Blackwell Scientific Publications, 57-72.

Technoexport, 1981. Detail geology prospecting in the Anarak Area Central Iran. Geological Survey of Iran, No 9, 154pp.

Waight, T.E., Weaver, S.D., Muir, R.J., 1998. The Hohonu batholith of north Westland, New Zealand; granitoid compositions controlled by source H_2O contents and generated during tectonic transition. Contributions to Mineralogy and Petrology, 130, 225-239.

Whalen, J.B., Currie, K.L., Chappell, B.W., 1987. A-type granites: geochemical characteristics, discrimination and petrogenesis. Contributions to Mineralogy and Petrology, 95, 407-419.

White, A.J.R., Chappell, B.W., 1988. Granites. In: Douglas, J.G., Ferguson, J.A. (eds.). Geology of Victoria. Melbourne, Geological Society of Australia, Victoria Division, 427-439.

Wiedenbeck, M., Alle, P., Corfu, F., Griffin, W.L., Meier, M., Oberli, F., Quadt, A.V., Roddick, J.C., Spiegel, W., 1995. Three natural zircon standards for U-Th-Pb, Lu-Hf, trace element and REE analyses. Geostandards and Geoanalytical Research, 19, 1-23.

Wilmsen, M., Fürsich, F.T., Seyed-Emami, K., Majidifard, M.R., Taheri, J., 2009. The Cimmerian Orogeny in northern Iran: tectono-stratigraphic evidence from the foreland. Terra Nova, 21, 211-218.

Wilson, M., 1989. Igneous Petrogenesis: A Global Tectonic Approach. Harper Collins Academic, 466pp.

Xie, G., Mao, J., Li, R., Zhou, S.h., Ye, H., Yan, Q., Zhang, Z., 2006. SHRIMP zircon U-Pb dating for volcanic rocks of the Dasi Formation in southeast Hubei Province, middle-lower reaches of the Yangtze River and its implications. Chinese Science Bulletin, 51, 3000-3009.

Zen, E.A., 1986. Aluminum enrichment in silicate melts by fractional crystallization, some mineralogical and petrographic constraints. Journal of Petrology, 27, 1095-1118.

Manuscript received October 2015;
revision accepted July 2016;
published Online February 2017.

ELECTRONIC APPENDIX I

TABLE I. Major and trace elements data from the Ardestan area (GK: Kuh-e Dom granodiorite, DK: Kuh-e Dom diorite, MH: Mehrabad granodiorite, NS: Nasrand granodiorite, ZF: Zafarghand granodiorite, FS: Feshark granodiorite) (Some of the data of Hamzehie, 2013; Ghahramani, 2013; Aliashrafzadeh, 2013)

Sample	GK1	GK2	GK3	GK4	GK5	GK6	GK7	GK8	GK9	GK10	GK11	GK12
Wt. %												
SiO_2	63.7	65	66.3	65.8	66.91	65.43	67.3	63.77	62.68	66.59	70.6	63.8
TiO_2	0.48	0.43	0.4	0.44	0.5	0.48	0.32	0.55	0.61	0.47	0.24	0.46
Al_2O_3	14.95	15.05	15.25	15.25	15.69	16	15.7	16.38	16.15	15.76	13.85	16
Fe_2O_3	1.79	1.79	1.67	1.78	1.24	2.17	1.47	2.22	2.51	1.94	1.14	1.38
FeO	2.38	2.28	2.02	2.17	1.34	2.37	1.59	2.58	2.83	2.36	1.37	1.83
MnO	0.09	0.07	0.07	0.11	0.06	0.09	0.04	0.08	0.08	0.06	0.03	0.09
MgO	1.44	1.68	1.22	1.43	1.36	1.65	0.9	1.59	2.11	1.68	0.79	1.97
CaO	3.61	2.84	2.66	3.12	4.11	2.91	2.12	4.28	4.13	3.26	2.01	3.08
Na_2O	3.11	3.16	3.22	3.33	3.85	3.76	3.28	3.53	3.23	3.62	3.37	5
K_2O	3.72	3.98	4.28	4.15	4.64	4.71	5.23	4.52	5.13	3.81	3.98	1.8
P_2O_5	0.15	0.12	0.1	0.13	0.15	0.15	0.09	0.19	0.19	0.15	0.03	0.13
Total	95.42	96.40	97.19	97.71	99.85	99.72	98.04	99.69	99.65	99.70	97.41	95.54
ppm												
Ce	56.3	100	65.8	56.6	45.5	39.4	61.4	47.3	55.6	46	65	46
Cr	60	70	50	40	10	0	10	20	16.6	10	10	10
Nb	14.7	14.5	15.1	13.9	15	12.93	19.9	17.2	16.16	13.9	14.5	14.8
Ni	5	5	4	4	6	4	5	9	9.1	6	8	8
Pb	11	12	11	10	8	10.1	10	12	9.1	10	14	*
Rb	122.5	146	154.5	122.5	117	156.8	147.5	146	185.5	111	143	73.2
Sr	263	295	249	247	354	279.1	197.5	395	340.4	276	218	312
Th	16.4	18.5	20.1	16.8	16.05	16.85	28.6	22.5	26.79	15.9	22.5	18.05
Y	17.8	19.3	17.2	17.7	18.5	22.7	17.9	19.1	25.3	16.2	18.4	18.2
Zr	164	160	186	160	180	171	161	171	187	179	125	182
Ba	560	685	569	534	648	526.5	519	589	498.3	577	567	290

TABLE I. Continued

Sample	DK1	DK2	DK3	DK4	DK5	DK6	DK7	DK8	DK9	DK10	DK11
Wt.%											
SiO_2	57.1	57.3	54.96	48.79	48.5	54.6	47.2	54.4	61.6	53	53.8
TiO_2	0.75	0.79	1.01	1.07	0.98	1	1.02	0.86	0.57	0.94	1.03
Al_2O_3	16.5	16.15	19.19	17.72	19.75	19.5	17.6	16.4	15.9	16.85	17.1
Fe_2O_3	1.50	2.31	2.75	2.70	2.74	2.34	2.11	2.03	2.15	1.35	3.37
FeO	2.02	4.48	4.21	3.49	4.32	3.95	4.09	3.38	2.74	2.12	5.03
MnO	0.1	0.13	0.1	0.35	0.19	0.13	0.13	0.14	0.09	0.21	0.18
MgO	2.57	3.82	3.75	2.21	2.36	2.81	4.91	4.04	1.68	5.1	4.37
CaO	8	6.64	7	14.91	8.76	8	12.45	8.16	4.78	11.35	7.2
Na_2O	3.29	3.39	3.56	2.42	3.13	3.95	3.1	4.56	3.48	4.21	3.18
K_2O	3.83	0.61	2.55	5.52	3.09	1.34	1.48	0.83	3.85	1.77	3.2
P_2O_5	0.24	0.24	0.41	0.41	0.39	0.54	0.47	0.34	0.15	0.36	0.41
Total	95.90	95.86	99.49	99.59	94.21	98.16	94.56	95.14	96.99	97.26	98.87
ppm											
Ce	61.1	62.3	50.2	53.9	52.8	68.6	49.7	68.1	61.7	57.7	79.3
Cr	40	90	30	118.2	30	66	210	200	20	80	80
Nb	18.4	17.4	13.8	8.54	13.8	31.8	11.7	22.2	19.8	24.6	27.8
Ni	13	26	13	27.8	15	32	69	69	11	24	37
Pb	13	7	14	8.8	11	21	9	6	12	*	*
Rb	114.5	24	93.4	184.3	113.5	62.7	75.5	35.1	146	73.1	135.5
Sr	525	460	692	430.6	518	672	725	460	354	733	583
Th	20.8	21.2	12.35	10.49	12.7	11.35	6.27	13.5	23.4	17.6	18.65
Y	25.4	22.6	20.1	25.8	23.4	27.6	22.4	26.5	27.4	23.5	26.8
Zr	193	197	137	91.2	119	195	85	211	207	245	294
Ba	619	110.5	424	374.4	460	208	280	123	546	356	454

TABLE I. Continued

Sample	MH1	MH2	MH3	MH4	MH5	MH6	MH7	MH8	MH9	MH10	MH11	MH12
Wt.%												
SiO_2	59.79	56.69	61.56	63.30	61.31	68.4	70.21	69.50	71.46	50.89	59.97	61.13
TiO_2	0.71	0.85	0.75	0.72	0.67	0.47	0.33	0.44	0.3	0.73	0.89	0.72
Al_2O_3	16.59	16.63	15.81	15.74	15.68	15.56	14.67	15.89	14.27	15.93	15.94	15.87
Fe_2O_3	2.79	3.00	2.60	2.46	3.12	1.07	1.37	0.51	1.47	2.65	3.30	2.86
FeO	4.50	5.37	4.19	3.67	3.84	1.74	1.58	0.72	1.54	5.56	4.49	4.24
MnO	0.14	0.14	0.11	0.10	0.35	0.06	0.04	0.04	0.04	0.14	0.13	0.13
MgO	2.93	4.11	2.84	2.29	2.49	1.98	0.98	1.89	0.82	8.08	3.29	3
CaO	6.49	7.74	6.22	5.25	4.24	5.64	2.79	4.83	1.32	11.56	4.36	5.36
Na_2O	3.47	2.98	3.34	3.82	4.15	4.04	3.00	5.12	3.36	3.15	3.88	3.29
K_2O	1.88	1.68	1.92	2.03	3.5	0.71	4.74	0.86	5.17	0.6	2.96	2.72
P_2O_5	0.17	0.17	0.17	0.19	0.19	0.12	0.08	0.12	0.07	0.05	0.22	0.17
Total	99.46	99.36	99.50	99.57	99.54	99.79	99.80	99.91	99.81	99.35	99.44	99.48
ppm												
Ce	26.2	22.8	27.3	31.2	21.1	36	32	19.1	37.3	4.4	29	29.2
Cr	10	30	20	20	10	10	5	5	10	200	20	20
Nb	3.8	3.5	3.9	5.1	2.7	6	4.5	4.9	5.5	0.6	5.1	4
Ni	4.4	12.8	9.1	4.9	7.6	0.1	0.2	2.3		78.6	9	8.8
Pb	6.7	5.6	6.4	8.5	9.1	5.2	5.6	4.7	8.1	2	17.5	8.3
Rb	41	41	42.6	50.4	89.3	31.4	114.5	26.2	133	8	83.9	73.5
Sr	310	341	302	307	257	619	338	678	279	282	317	348
Th	3.59	2.78	3.79	3.72	2.09	16.4	9.08	8.72	13.25	0.09	4.14	4.45
Y	30.6	24.9	28.3	31.4	24.1	23.5	15.8	17.9	17	18.4	32.1	29.7
Zr	130	90	140	140	100	150	160	180	190	40	150	150
Ba	419	347	428	466	751	150.5	765	250	783	55.9	695	588

TABLE I. Continued

Sample	MH13	MH14	NS1	NS2	NS3	NS4	NS5	NS6	ZF1	ZF2	ZF3	ZF4
Wt.%												
SiO_2	70.55	62.78	70.42	74.07	77.88	71.89	71.22	70.08	77.56	55.15	58.61	75.93
TiO_2	0.4	0.77	0.36	0.27	0.16	0.28	0.34	0.43	0.11	1.18	0.88	0.33
Al_2O_3	15.38	16.06	14.31	13.92	12.53	13.46	14.64	14.52	12.14	17.1	16.38	13.01
Fe_2O_3	0.66	2.35	1.49	0.53	0.34	1.08	0.87	1.54	0.61	2.94	3.22	0.41
FeO	0.79	3.77	1.60	0.52	0.39	1.49	0.89	1.68	0.64	5.87	4.45	0.49
MnO	0.06	0.11	0.05	0.03	0.02	0.04	0.03	0.07	0.02	0.23	0.2	0.02
MgO	1.55	2.55	0.83	0.36	0.19	0.03	0.7	0.91	0.11	4.14	5.18	0.55
CaO	3.09	5.73	2.31	1.23	1.08	5.48	2.39	2.21	0.62	8.56	3.56	2.13
Na_2O	6.41	3.58	3.38	4.03	3.64	2.97	3.55	3.74	3.72	3.33	4.21	6.75
K_2O	0.92	1.64	4.97	4.94	3.74	3.04	5.18	4.5	4.39	0.55	2.57	0.24
P_2O_5	0.1	0.22	0.09	0.05	0.01	0.06	0.08	0.1	0.01	0.28	0.19	0.07
Total	99.90	99.56	99.80	99.95	99.98	99.82	99.89	99.78	99.93	99.33	99.45	99.93
ppm												
Ce	27.2	31.6	80.8	25	23.4	82.2	52.7	72.3	58.9	43.8	46.3	41.4
Cr	*	*	10	*	8	10	10	10	10	50	20	10
Nb	3.8	4.3	14.3	12.3	15.5	20.4	14.6	16.3	9.8	9.6	8.9	9.8
Ni	1.1	3	*	*	*	*	*	*	*	25.7	8.1	2.4
Pb	7	6.4	8.7	3.7	3.3	6.7	6.4	9.3	8.1	6.2	5.4	1.4
Rb	27.2	50.5	161	139.4	119.5	253	148	165	123.5	13.5	64.2	5.2
Sr	483.7	439.6	194	172.3	178	47.5	234	194	43.2	348	252	161.5
Th	8.9	8.7	28.9	25	35.3	54.6	31.4	23.2	15	3.96	8.04	14.55
Y	16.3	22.3	29.1	27.7	23	42.3	25.9	32.8	45.1	37.7	25.4	46.7
Zr	146.7	122.6	260	139.3	130	150	210	290	170	240	160	270
Ba	132.4	283.3	822	715.9	666	151.5	986	808	1215	404	610	40.6

TABLE I. Continued

Sample	ZF5	ZF6	ZF7	ZF8	FS1	FS2	FS3	FS4	FS5	FS6	FS7
Wt.%											
SiO_2	52.01	54.29	73.72	52.25	64.19	66.95	58.74	54.17	77.53	58.58	59.43
TiO_2	1.51	1.26	0.55	1.04	0.68	0.6	0.8	0.91	0.13	0.81	0.75
Al_2O_3	15.79	17.94	13.52	16.55	15.48	15.3	16.66	17.08	11.98	16.19	17.29
Fe_2O_3	3.70	3.02	0.88	3.14	2.24	1.62	2.81	3.23	0.61	2.92	2.45
FeO	7.59	5.66	1.27	5.72	3.47	2.45	4.69	6.99	0.67	4.91	4.13
MnO	0.17	3.53	0.81	6.21	0.1	0.05	0.13	0.19	0.02	0.1	0.11
MgO	5.34	8.66	3.46	9.24	2.45	1.94	3.4	4.7	0.25	3.75	3.14
CaO	8.93	3.64	5.18	4.25	5.42	5.19	6.93	8.49	1.05	6.93	7.08
Na_2O	3.13	0.79	0.35	0.54	3.33	5.25	3.36	2.75	2.41	4.17	3.51
K_2O	0.71	0.35	0.1	0.35	2.11	0.24	1.77	0.56	5.25	0.92	1.51
P_2O_5	0.24	0.19	0.03	0.05	0.13	0.11	0.15	0.1	0.02	0.13	0.11
Total	99.12	99.33	99.87	99.33	99.60	99.71	99.44	99.18	99.92	99.41	99.51
ppm											
Ce	28.6	34.1	48.8	39.3	35	29.1	36.6	14.6	24.7	32.6	28
Cr	70	20.8	*	138	3.7	*	4.5	2.5	*	9.9	11.5
Nb	6.7	7.1	10.3	7.7	6.9	6.2	6.6	2.4	2.7	5.1	4.8
Ni	47.5	11.9	1.9	54.9	4.1	2.1	4.6	2.7	*	5.3	2.9
Pb	4	19.5	2.2	1.7	7.9	4.5	8.1	7.4	9.2	4.7	5.1
Rb	25.8	20.3	12.4	13	69.9	7.1	62.1	19.3	128.3	33.5	49.3
Sr	342	336.6	254.4	385.5	245.6	220.6	281.4	332.6	75.9	243.4	270.6
Th	2.67	3.7	19.3	1.4	7.3	7	10.4	0.8	14.9	4.8	6.4
Y	31.5	23.9	30.1	18.4	22.3	21.2	23.3	17.4	16.8	22.1	20
Zr	110	158.1	303.5	108.5	166.7	137	122.5	53.5	100.8	81.2	167.7
Ba	275	346.5	96.9	128.7	375.7	89.7	361.6	156.5	494.4	219.7	303.2

TABLE II. U-Th-Pb data for the intrusive rocks of Ardestan area. (GK: Kuh-e Dom granodiorite, DK: Kuh-e Dom diorite, MH: Mehrabad granodiorite, NS: Nasrand granodiorite, ZF: Zafarghand granodiorite, FS: Feshark granodiorite)

Sample	Pb	Th^{232}	U^{238}	Th/U	$^{207}Pb/^{206}Pb$	$^{207}Pb/^{206}Pb$	$^{207}Pb/^{235}U$	$^{207}Pb/^{235}U$	$^{206}Pb/^{238}U$	$^{206}Pb/^{238}U$	
	ppm	ppm	ppm		Ratio	1sigma	Ratio	1sigma	Ratio	1sigma	rho
GK-01	4.13	258	388	0.67	0.0764	0.0054	0.0858	0.0066	0.0080	0.0002	0.2688
GK-02	2.06	96.1	221	0.44	0.0718	0.0066	0.0714	0.0057	0.0080	0.0002	0.3410
GK-03	4.70	304	483	0.63	0.0491	0.0033	0.0532	0.0034	0.0080	0.0001	0.2703
GK-04	4.15	301	431	0.70	0.0534	0.0046	0.0582	0.0052	0.0080	0.0002	0.2341
GK-05	1.95	99.1	202	0.49	0.0834	0.0073	0.0847	0.0064	0.0080	0.0002	0.3493
GK-06	2.84	169	311	0.54	0.0591	0.0044	0.0634	0.0048	0.0080	0.0002	0.3364
GK-07	2.29	104	254	0.41	0.0621	0.0066	0.0651	0.0065	0.0080	0.0002	0.2550
GK-08	3.78	245	401	0.61	0.0573	0.0053	0.0585	0.0050	0.0078	0.0002	0.2832
GK-09	4.39	296	431	0.69	0.0545	0.0049	0.0583	0.0047	0.0082	0.0002	0.2303
GK-10	9.02	889	840	1.06	0.0509	0.0032	0.0556	0.0033	0.0079	0.0001	0.2398
GK-11	11.71	971	1126	0.86	0.0540	0.0030	0.0594	0.0033	0.0080	0.0001	0.2321
GK-12	8.82	767	769	1.00	0.0656	0.0049	0.0743	0.0055	0.0082	0.0001	0.2149
GK-13	4.90	252	514	0.49	0.0578	0.0050	0.0602	0.0049	0.0079	0.0001	0.2193
GK-14	3.01	142	323	0.44	0.0626	0.0050	0.0669	0.0053	0.0079	0.0002	0.2715
GK-15	4.43	319	460	0.69	0.0591	0.0052	0.0617	0.0054	0.0077	0.0002	0.2374
GK-16	5.83	409	600	0.68	0.0549	0.0040	0.0572	0.0038	0.0077	0.0001	0.2896
GK-17	3.19	152	320	0.47	0.0619	0.0049	0.0700	0.0053	0.0083	0.0002	0.3059
GK-18	2.72	134	285	0.47	0.0643	0.0055	0.0703	0.0061	0.0080	0.0002	0.2761
GK-19	2.71	144	307	0.47	0.0584	0.0051	0.0621	0.0054	0.0080	0.0002	0.2509
GK-21	7.27	490	766	0.64	0.0514	0.0029	0.0545	0.0029	0.0077	0.0001	0.2488
GK-22	3.09	136	311	0.44	0.0664	0.0045	0.0731	0.0048	0.0082	0.0002	0.3744
GK-23	6.17	456	628	0.73	0.0559	0.0042	0.0594	0.0041	0.0079	0.0001	0.2181
GK-24	3.26	191	333	0.57	0.0758	0.0068	0.0805	0.0069	0.0080	0.0002	0.2473
DK-01	5.64	454	523	0.87	0.0507	0.0023	0.0566	0.0025	0.0082	0.0001	0.2641
DK-02	5.77	404	555	0.73	0.0468	0.0022	0.0522	0.0024	0.0082	0.0001	0.2444
DK-03	8.88	709	815	0.87	0.0466	0.0020	0.0526	0.0022	0.0082	0.0001	0.2285
DK-04	9.98	777	895	0.87	0.0488	0.0018	0.0569	0.0021	0.0085	0.0001	0.2699
DK-05	26.86	1795	2531	0.71	0.0467	0.0011	0.0547	0.0013	0.0085	0.0001	0.3647
DK-06	10.21	829	914	0.91	0.0465	0.0018	0.0547	0.0021	0.0085	0.0001	0.3267
DK-07	7.75	595	731	0.81	0.0472	0.0019	0.0536	0.0022	0.0082	0.0001	0.2584
DK-08	9.30	734	829	0.88	0.0491	0.0022	0.0573	0.0026	0.0084	0.0001	0.2350
DK-09	6.92	460	651	0.71	0.0460	0.0022	0.0533	0.0025	0.0085	0.0001	0.2088
DK-10	7.64	617	678	0.91	0.0471	0.0020	0.0549	0.0023	0.0085	0.0001	0.2890
DK-12	26.3	2192	2351	0.93	0.0462	0.0011	0.0538	0.0013	0.0085	0.0001	0.4858
DK-13	29.51	1213	2994	0.41	0.0473	0.0011	0.0548	0.0012	0.0084	0.0001	0.3764
DK-14	8.48	654	763	0.86	0.0498	0.0026	0.0577	0.0029	0.0085	0.0001	0.1915
DK-15	45.7	2615	4259	0.61	0.0494	0.0010	0.0582	0.0012	0.0085	0.0001	0.4238
NS_01	20.3	471	1504	0.31	0.0968	0.0105	0.0746	0.0079	0.0056	0.0001	0.1450
NS_02	2.48	211	367	0.57	0.0622	0.0060	0.0450	0.0039	0.0057	0.0002	0.3128
NS_03	1.88	141	245	0.57	0.1239	0.0139	0.0904	0.0096	0.0057	0.0002	0.2785
NS_04	2.51	178	352	0.50	0.0742	0.0093	0.0528	0.0060	0.0057	0.0002	0.2355
NS_05	1.32	109	191	0.57	0.0786	0.0198	0.0471	0.0066	0.0056	0.0002	0.2342
NS_06	5.81	468	785	0.60	0.0861	0.0064	0.0659	0.0048	0.0056	0.0001	0.2095
NS_07	5.27	403	718	0.56	0.0843	0.0063	0.0679	0.0048	0.0058	0.0001	0.3227
NS_08	2.40	187	286	0.65	0.1206	0.0146	0.0870	0.0093	0.0057	0.0002	0.2699
NS_09	3.09	239	384	0.62	0.1182	0.0115	0.0940	0.0096	0.0057	0.0001	0.2477
NS_10	1.78	151	220	0.68	0.1187	0.0137	0.0836	0.0078	0.0058	0.0002	0.3547
NS_11	4.83	416	715	0.58	0.0473	0.0046	0.0365	0.0037	0.0057	0.0001	0.2385
MH_01	2.18	218	286	0.76	0.0737	0.0064	0.0606	0.0050	0.0057	0.0001	0.3048
MH_02	3.01	257	368	0.70	0.1294	0.0129	0.0899	0.0075	0.0057	0.0002	0.3851
MH_03	12.10	2035	1354	1.50	0.0495	0.0037	0.0382	0.0026	0.0057	0.0001	0.2237
MH_04	13.06	2116	1467	1.44	0.0477	0.0040	0.0370	0.0028	0.0058	0.0001	0.2825
MH_05	2.59	267	330	0.81	0.0759	0.0085	0.0563	0.0056	0.0057	0.0001	0.2434
MH_06	4.89	524	648	0.81	0.0498	0.0041	0.0380	0.0029	0.0057	0.0001	0.2367
MH_07	1.59	130	228	0.57	0.0934	0.0109	0.0690	0.0073	0.0058	0.0002	0.2958
MH_08	1.75	120	244	0.49	0.0894	0.0098	0.0647	0.0058	0.0057	0.0002	0.2975
MH_11	3.92	470	502	0.94	0.0478	0.0051	0.0374	0.0037	0.0057	0.0001	0.2145
MH_12	1.09	85.8	166	0.52	0.0792	0.0197	0.0487	0.0061	0.0057	0.0002	0.3218

TABLE II. Continued

Sample	Pb ppm	Th^{232} ppm	U^{238} ppm	Th/U	$^{207}Pb/^{206}Pb$ Ratio	$^{207}Pb/^{206}Pb$ 1sigma	$^{207}Pb/^{235}U$ Ratio	$^{207}Pb/^{235}U$ 1sigma	$^{206}Pb/^{238}U$ Ratio	$^{206}Pb/^{238}U$ 1sigma	rho
ZF_01	0.47	40.7	83.1	0.49	1.1361	0.4612	0.1638	0.0172	0.0038	0.0002	0.5844
ZF_02	1.53	231	263	0.88	0.1104	0.0156	0.0520	0.0063	0.0041	0.0001	0.2925
ZF_04	1.29	210	257	0.82	0.0970	0.0142	0.0454	0.0062	0.0039	0.0001	0.2391
ZF_05	0.66	63.5	112	0.57	0.4159	0.1342	0.1112	0.0146	0.0041	0.0003	0.4923
ZF_06	0.37	42.8	88.8	0.48	0.2869	0.0664	0.0918	0.0121	0.0036	0.0002	0.4152
ZF_08	1.32	255	251	1.02	0.0536	0.0106	0.0266	0.0050	0.0038	0.0002	0.2484
ZF_09	0.88	80.6	162	0.50	0.6727	0.4692	0.0776	0.0080	0.0038	0.0002	0.3921
ZF_10	0.44	45.9	105	0.44	0.2381	0.0699	0.0740	0.0136	0.0037	0.0002	0.3286
ZF_11	0.67	69.0	131	0.53	0.3338	0.1083	0.0924	0.0099	0.0038	0.0002	0.4249
ZF_12	1.40	166	306	0.54	0.1179	0.0114	0.0536	0.0049	0.0037	0.0001	0.3493
ZF_13	1.03	154	215	0.72	0.1363	0.0193	0.0605	0.0074	0.0038	0.0001	0.2741
ZF_14	0.55	56.9	116	0.49	0.1133	0.0189	0.0484	0.0068	0.0039	0.0002	0.3050
ZF_15	2.00	410	349	1.18	0.1054	0.0106	0.0482	0.0044	0.0038	0.0001	0.3083
FS_01	0.88	208	203	1.02	0.0331	0.0141	0.0238	0.0073	0.0032	0.0002	0.1882
FS_03	0.50	99.0	113	0.88	0.0000	0.0000	0.0578	0.0106	0.0031	0.0002	0.3577
FS_05	0.48	60.3	133	0.45	0.3650	0.2457	0.0485	0.0059	0.0032	0.0002	0.4048
FS_06	0.199	18.4	56.1	0.33	0.6247	0.1521	0.0766	0.0117	0.0032	0.0003	0.5500
FS_07	0.90	178	230	0.77	0.1119	0.0236	0.0330	0.0042	0.0032	0.0001	0.3147
FS_10	0.93	127	252	0.50	0.1084	0.0131	0.0431	0.0043	0.0031	0.0001	0.4398
FS_12	0.52	70.4	123	0.57	0.2894	0.0753	0.0681	0.0079	0.0032	0.0002	0.4522
FS_15	0.35	58.9	96.4	0.61	0.8626	0.2674	0.0765	0.0126	0.0032	0.0002	0.4627

TABLE II. Continued

Sample	$^{208}Pb/^{232}Th$ Ratio	$^{208}Pb/232Th$ 1sigma	$^{238}U/^{232}Th$ Ratio	$^{207}Pb/^{206}Pb$ Age (Ma)	$^{207}Pb/^{206}Pb$ 1sigma	$^{207}Pb/^{235}U$ Age (Ma)	$^{207}Pb/^{235}U$ 1sigma	$^{206}Pb/^{238}U$ Age (Ma)	$^{206}Pb/^{238}U$ 1sigma	$^{208}Pb/^{232}Th$ Age (Ma)	$^{208}Pb/^{232}Th$ 1sigma
GK-01	0.0034	0.0001	1.5972	1106	138	83.6	6.1	51.5	1.1	67.7	2.8
GK-02	0.0029	0.0002	2.4262	981	192	70.1	5.4	51.2	1.4	57.9	4.8
GK-03	0.0027	0.0001	1.7365	154	148	52.6	3.3	51.6	0.9	55.2	2.7
GK-04	0.0024	0.0001	1.5277	346	194	57.5	5.0	51.1	1.1	49.1	2.4
GK-05	0.0032	0.0002	2.1829	1280	171	82.5	6.0	51.6	1.4	63.8	4.2
GK-06	0.0024	0.0002	2.0671	569	163	62.5	4.6	51.2	1.3	49.0	3.3
GK-07	0.0029	0.0002	2.5888	680	234	64.0	6.2	51.3	1.3	57.9	3.8
GK-08	0.0025	0.0001	1.7332	502	204	57.8	4.8	50.3	1.2	51.4	2.5
GK-09	0.0028	0.0001	1.5768	391	206	57.6	4.5	52.5	1.0	57.5	2.4
GK-10	0.0026	0.0001	1.0709	239	153	55.0	3.2	50.9	0.7	52.1	1.7
GK-11	0.0027	0.0001	1.3203	372	126	58.6	3.2	51.1	0.7	54.5	1.7
GK-12	0.0031	0.0001	1.0839	792	157	72.8	5.2	52.9	0.8	63.1	2.1
GK-13	0.0032	0.0005	2.1594	524	191	59.3	4.7	50.5	0.9	64.7	10.3
GK-14	0.0029	0.0002	2.4132	694	168	65.7	5.0	50.8	1.1	58.1	3.4
GK-15	0.0027	0.0001	1.5334	569	193	60.8	5.2	49.6	1.0	53.5	2.6
GK-16	0.0028	0.0001	1.7750	409	167	56.5	3.6	49.8	1.0	56.5	3.0
GK-17	0.0034	0.0002	2.2404	672	166	68.7	5.1	53.4	1.2	68.3	4.0
GK-18	0.0032	0.0002	2.2516	754	181	69.0	5.8	51.3	1.2	64.4	4.4
GK-19	0.0019	0.0001	2.2674	546	194	61.2	5.1	51.5	1.1	39.2	2.8
GK-21	0.0027	0.0001	1.6779	261	128	53.8	2.8	49.7	0.7	54.5	1.8
GK-22	0.0035	0.0002	2.4326	820	141	71.6	4.5	52.9	1.3	70.6	4.9
GK-23	0.0026	0.0001	1.4657	456	167	58.6	4.0	50.6	0.8	52.9	1.8
GK-24	0.0029	0.0002	1.8637	1100	180	78.6	6.5	51.2	1.1	58.9	4.0
DK-01	0.0026	0.0001	1.1562	233	106	55.9	2.4	52.4	0.6	53.0	1.3
DK-02	0.0027	0.0001	1.3632	39	111	51.7	2.3	52.3	0.6	54.2	1.5
DK-03	0.0028	0.0001	1.1377	31.6	100.0	52.1	2.2	52.7	0.5	57.2	1.3
DK-04	0.0028	0.0001	1.1421	139	89	56.2	2.0	54.5	0.5	57.5	1.1
DK-05	0.0030	0.0001	1.4411	31.6	55.6	54.1	1.3	54.3	0.5	59.8	1.0
DK-06	0.0030	0.0001	1.0870	33.43	88.9	54.1	2.1	54.8	0.7	61.0	1.4
DK-07	0.0027	0.0001	1.2384	58	96	53.0	2.1	52.9	0.5	54.3	1.3
DK-08	0.0030	0.0001	1.1131	150	104	56.6	2.5	54.2	0.6	60.7	1.3
DK-09	0.0027	0.0001	1.4006	*		52.7	2.4	54.3	0.5	55.4	1.3
DK-10	0.0028	0.0001	1.0737	53.8	100.0	54.3	2.2	54.7	0.7	56.8	1.2
DK-12	0.0028	0.0001	1.0926	5.66	55.6	53.2	1.2	54.3	0.6	56.6	1.1
DK-13	0.0026	0.0000	2.4407	64.9	51.8	54.2	1.2	53.9	0.4	53.4	1.0
DK-14	0.0025	0.0001	1.1361	187	122	57.0	2.8	54.3	0.5	50.6	1.2
DK-15	0.0028	0.0000	1.5815	169	46	57.5	1.1	54.8	0.5	56.4	0.9
NS_01	0.0040	0.0003	3.2681	1565	203.7	73	7.5	36.1	0.6	81	6.7
NS_02	0.0019	0.0001	1.7937	681	206	44.7	3.8	36.3	1.0	38.3	2.6
NS_03	0.0030	0.0002	1.7951	2013	206	88	8.9	36.9	1.1	61.0	4.8
NS_04	0.0025	0.0002	2.1014	1056	256	52.2	5.8	36.5	1.0	50.2	3.0
NS_05	0.0026	0.0002	1.8141	1163	514	46.7	6.4	36.3	1.2	52.9	3.8
NS_06	0.0023	0.0001	1.7624	1340	143	64.8	4.6	36.3	0.6	47.0	3.0
NS_07	0.0028	0.0002	1.7594	1302	144.4	66.7	4.6	37.3	0.9	56.4	3.5
NS_08	0.0030	0.0002	1.7938	1966	218.1	84.7	8.7	36.8	1.1	61.2	4.8
NS_09	0.0033	0.0003	1.6766	1929	175	91	8.9	36.3	0.9	68	6.2
NS_10	0.0027	0.0002	1.5674	1939	207	81.6	7.3	37.4	1.2	54.7	4.2
NS_11	0.0017	0.0001	1.8552	61	218	36.4	3.6	36.5	0.9	34.1	2.3
MH_01	0.0020	0.0001	1.4148	1035	175	59.8	4.8	36.8	0.9	41.4	2.3
MH_02	0.0027	0.0002	1.4880	2090	177.0	87	7.0	36.6	1.2	53.6	3.8
MH_03	0.0019	0.0001	0.6940	172	172	38.1	2.5	36.9	0.6	38.7	1.1
MH_04	0.0021	0.0001	0.7391	83	250.0	36.9	2.7	37.1	0.8	42.2	1.3
MH_05	0.0022	0.0001	1.4289	1092	226	55.6	5.4	36.7	0.9	45.4	2.7
MH_06	0.0019	0.0001	1.2888	183	181	37.9	2.9	36.8	0.7	39.1	1.5
MH_07	0.0021	0.0002	1.8126	1495	222	67.8	6.9	37.1	1.2	41.6	3.6
MH_08	0.0026	0.0001	2.1190	1413	212	63.7	5.5	36.5	1.0	53.1	2.9
MH_11	0.0023	0.0001	1.0979	87	237	37.3	3.7	36.8	0.8	46.8	2.2
MH_12	0.0024	0.0002	1.9919	1177	511	48.3	5.9	36.6	1.5	48.0	4.8
ZF_01	0.0040	0.0004	2.1053	*	*	154	15.0	24.7	1.5	80.7	7.1
ZF_02	0.0020	0.0001	1.1678	1806	259.6	51.5	6.1	26.4	0.9	39.9	2.7
ZF_04	0.0016	0.0001	1.2766	1569	277	45.1	6.0	24.8	0.8	31.7	2.3
ZF_05	0.0041	0.0004	1.8990	3968	505	107	13.4	26.1	1.7	83.5	8.0
ZF_06	0.0035	0.0003	2.1598	3401	369	89.1	11.3	23.0	1.3	69.9	6.6
ZF_08	0.0016	0.0001	1.0648	354	394	26.7	5.0	24.7	1.2	31.6	2.7
ZF_09	0.0031	0.0003	2.1477	4673	1819	75.9	7.5	24.7	1.0	61.7	5.9
ZF_10	0.0033	0.0003	2.3969	3107	485	72.5	12.8	23.6	1.4	66.0	6.3
ZF_11	0.0026	0.0002	1.9617	3635	519	89.7	9.2	24.2	1.1	52.5	4.6

TABLE II. Continued

Sample	$^{208}Pb/^{232}Th$ Ratio	$^{208}Pb/232Th$ 1sigma	$^{238}U/^{232}Th$ Ratio	$^{207}Pb/^{206}Pb$ Age (Ma)	$^{207}Pb/^{206}Pb$ 1sigma	$^{207}Pb/^{235}U$ Age (Ma)	$^{207}Pb/^{235}U$ 1sigma	$^{206}Pb/^{238}U$ Age (Ma)	$^{206}Pb/^{238}U$ 1sigma	$^{208}Pb/^{232}Th$ Age (Ma)	$^{208}Pb/^{232}Th$ 1sigma
ZF_12	0.0017	0.0001	2.3132	1924	173	53.0	4.7	23.8	0.8	34.2	2.9
ZF_13	0.0012	0.0001	1.4815	2181	249	59.6	7.1	24.5	0.8	24.5	2.4
ZF_14	0.0022	0.0002	2.1421	1854	306	48.0	6.5	24.9	1.1	45.3	4.4
ZF_15	0.0014	0.0001	0.8827	1722	187	47.8	4.3	24.4	0.7	29.2	1.7
FS_01	0.0017	0.0002	1.2271	*	*	23.9	7.2	20.8	1.2	34.1	3.7
FS_03	0.0021	0.0002	1.1936	*	*	57.1	10.2	20.1	1.3	43.3	3.9
FS_05	0.0019	0.0002	2.3017	3771	1294	48.0	5.7	20.3	1.0	38.5	4.2
FS_06	0.0049	0.0006	3.2029	4567	409	75.0	11.0	20.6	1.7	98.1	12.4
FS_07	0.0011	0.0001	1.3537	1831	391	33.0	4.2	20.5	0.8	22.7	2.0
FS_10	0.0012	0.0002	2.0605	1773	222	42.9	4.2	20.3	0.9	24.2	3.6
FS_12	0.0017	0.0002	1.8118	3415	417	66.9	7.6	20.8	1.1	34.0	4.0
FS_15	0.0022	0.0003	1.6987	*	*	74.8	11.8	20.6	1.6	44.4	5.6

TABLE III. U-Pb data for intrusive rocks in the Ardestan area

Locality	Number of sites	Type rocks	Age	MSWD	Figure
Kuh-e Dom		diorite	53.90 ±0.40Ma	1.18	9A
Kuh-e Dom	37	granodiorite	51.10±0.40Ma	1.04	9B
Mehrabad	10	granodiorite	36.8±0.5Ma	0.047	9C
Nasrand	11	granodiorite	36.5±0.5Ma	0.23	9D
Zafarghand	13	granodiorite	24.6±0.5Ma	0.66	9E
Feshark	8	granodiorite	20.5±0.8Ma	0.045	9F

MSWD: Mean Squared Weighted Deviates

TABLE IV. Some reported radiometric ages of UDMA plutonic rocks

Locality	Type rocks	Age (Ma)	Epoch	Reference
Shir-Kuh	granodiorite-diorite	166.0-166.8	Middle Jurassic	Chiu *et al.*, 2013
Bazman area	gabbro to granite	81–72	Late Cretaceous	Chiu *et al.*, 2014
Bam-Jiroft	gabbro	76.6	Late Cretaceous	Chiu *et al.*, 2015
Mozvash at the Kashan	microdiorite	50.1	Early Eocene	Honarmand *et al.*, 2013
Khalkhab- Siljerd at the Saveh	monzogabbro/diorite,granodiorite	36.6–40.3	Upper Eocene	Rezaei *et al.*, 2011
between Kashan and Natanz	microdiorite	33	Oligocene	Chiu *et al.*, 2013
Rigan near Bam	granitic rocks	29	Oligocene	McInnes *et al.*, 2003
Bam-Jiroft areas	diorite	29.9	upper Oligocene	Chiu *et al.*, 2013
South of Kerman	diorite	30–24	Upper Oligocene	Chiu *et al.*, 2013
Natanz area	granitic rocks	21.2–19.6	Miocene	Chiu *et al.*, 2013
Ghalhar, Niyasar, and Poudalg	diorite	18.21	Lower-Middle Miocene	Honarmand *et al.*, 2013
between Kashan and Natanz	diorite	16	Middle Miocene	Chiu *et al.*, 2013
southwest of Qom	granodiorite	17.4	Middle Miocene	Chiu *et al.*, 2013
Anar-Sirjan-Kerman	granodiorite, diorite	9.4–5.4	Upper Miocene	Chiu *et al.*, 2013